Ni/Co doped 1T/2H MoS_2 as a robust bifunctional electrocatalyst for hydrogen and oxygen evolution in both acidic and alkaline media

Praveena Gurusamy[a], Kannan Nagarajan[a], Sundara Venkatesh Perumalsamy[a], Thamilmaran Pandia[a], Jeganathan Kulandaivel[b], K.M. Mithra[c], Rajkamal Anand[d], and S. Sinthika[e]

[1] Nanomaterials Laboratory, Department of Physics, Sri S. Ramasamy Naidu Memorial College, Sattur – 626 203, Tamil Nadu, India (Affiliated to Madurai Kamaraj University, Madurai – 625 021, Tamil Nadu, India).

[2] Centre for Nanoscience and Nanotechnology, Department of Physics, Bharathidasan University, Tiruchirappalli – 620 024, Tamil Nadu, India.

[4] Department of Physics and Research Centre, Lady Doak College, Madurai-625 002, Tamil Nadu, India (Affiliated to Madurai Kamaraj University, Madurai-625 021, Tamil Nadu, India).

[5] Institute of Advanced Aerospace Technology, Seoul National University, Gwanak-gu Gwanak-ro 1, Seoul 08826, Republic of Korea.

Table S1. The calculated average particle size and interlayer distance (d) of MDS and X-MDS samples.

Name of the catalysts	Average size of the particles (nm)	Interlayer distance (d) (nm)
MDS	86	0.0948
C-MDS	58	0.0950
Ni-MDS	42	0.0952
CN-MDS	39	0.0954

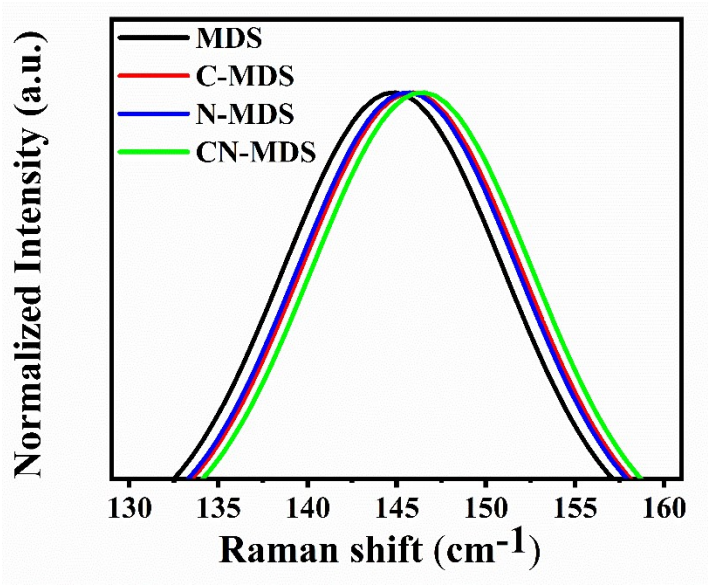

Fig. S1 Normalised zoomed-in Raman spectra of the J_1 mode of MDS and X-MDS NPs.

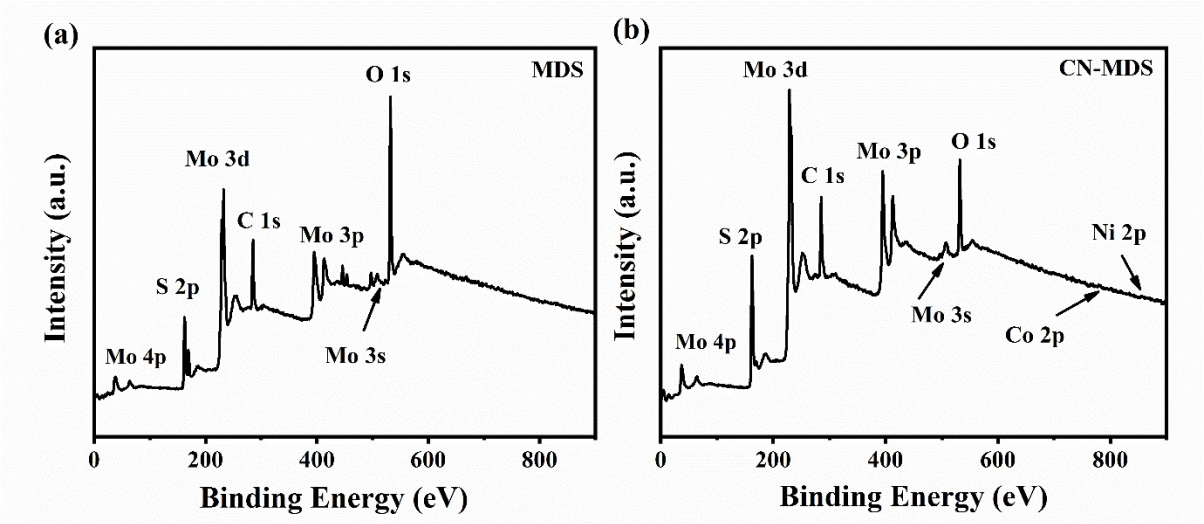

Fig. S2 XPS full survey scan spectra of (a) MDS and (b) CN-MDS.

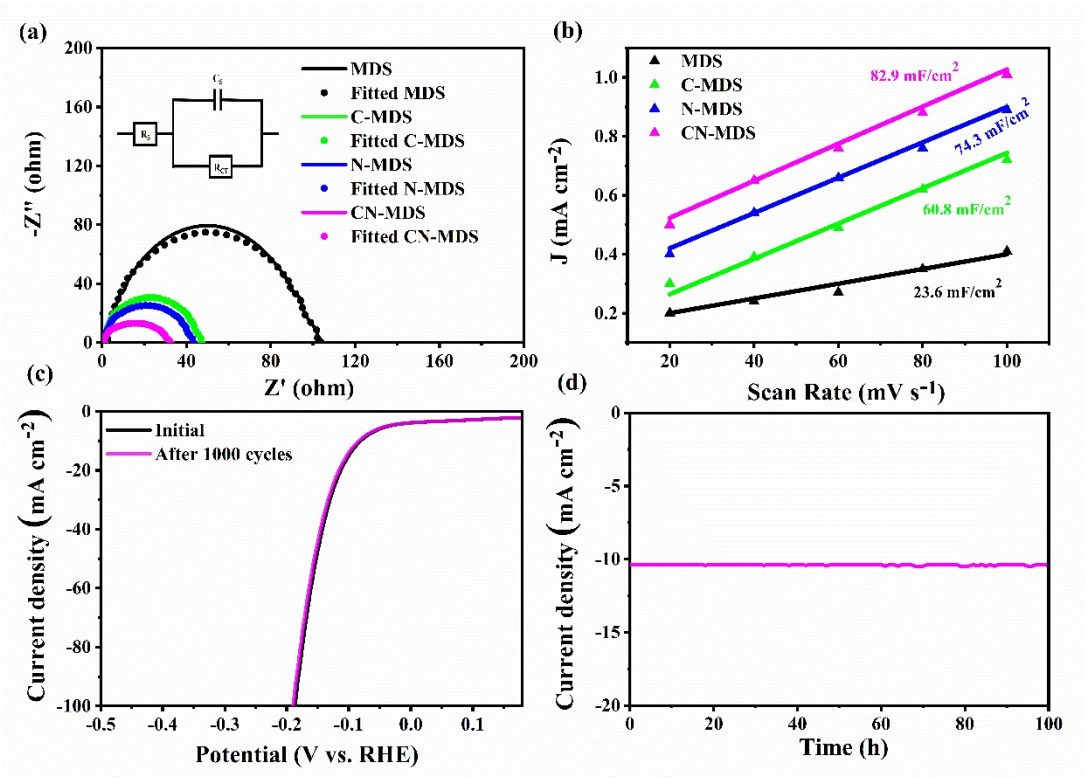

Fig. S3 Electrocatalytic HER studies of MDS and X-MDS in acid medium (a) Nyquist plots, (b) ECSA calculations using plots of scan rate vs current density, (c) Before and after 1000 cycles of CN-MDS polarisation curves at a scan rate of 5 mV/s, and (d) Current density-time (J-T) curve of CN-MDS for 100 h.

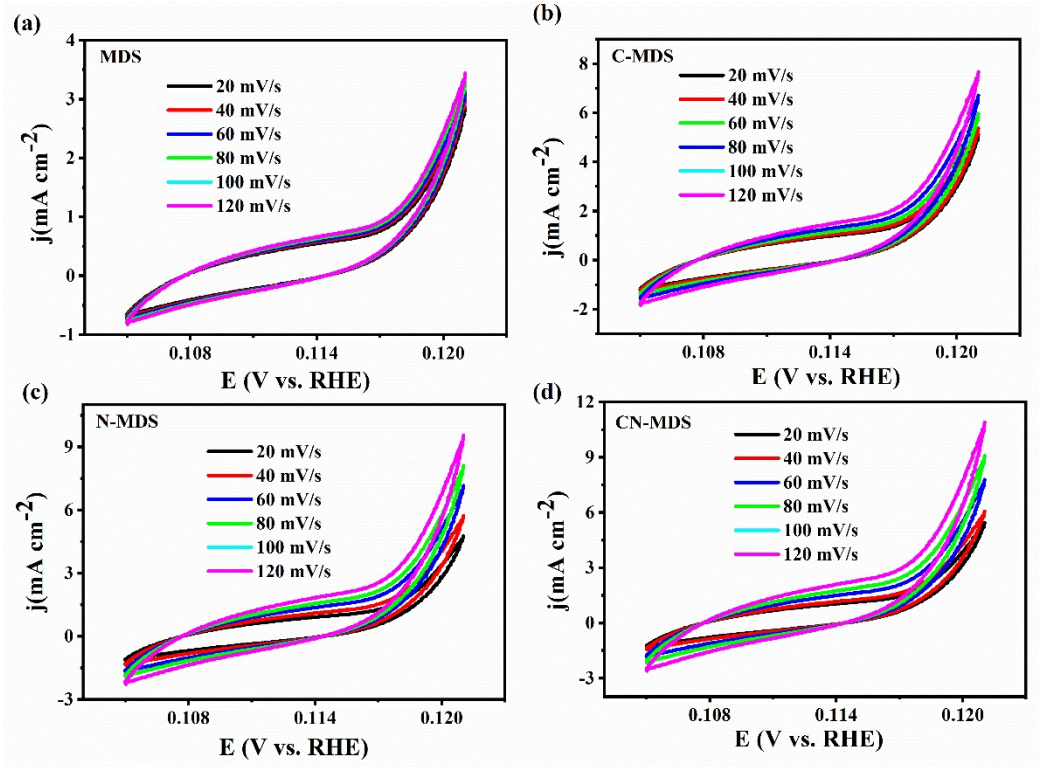

Fig. S4 Cyclic voltammograms for HER (a) MDS, (b) C-MDS, (c) N-MDS, and (d) CN-MDS in acid medium with the various scan rates.

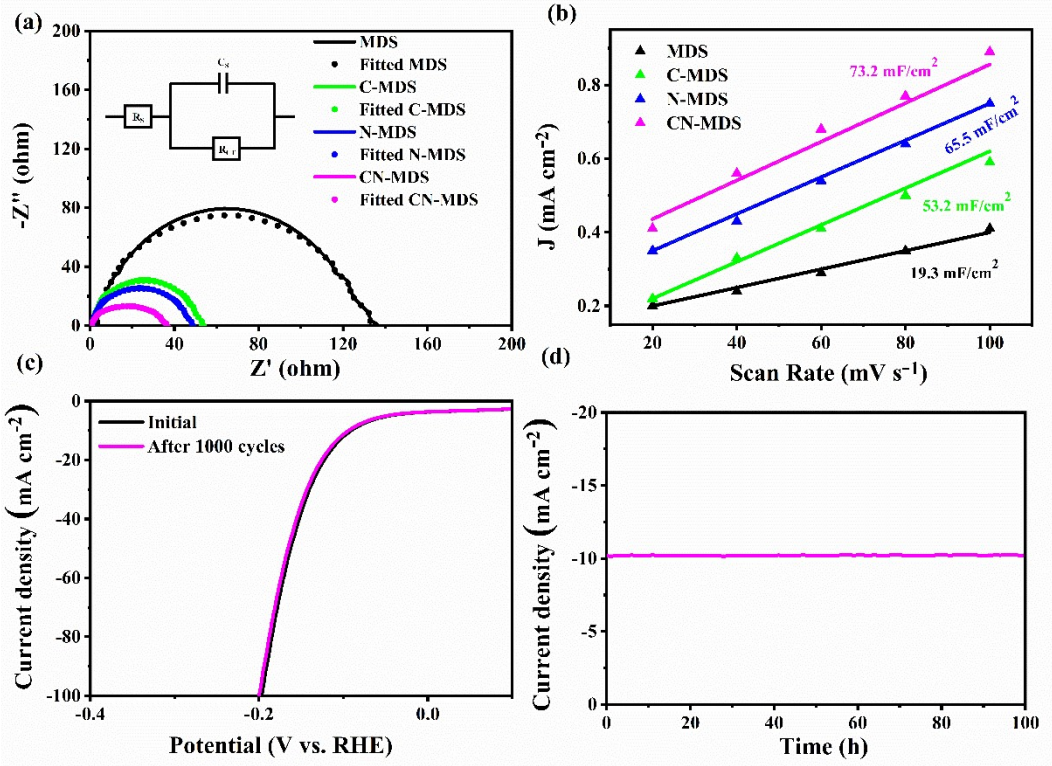

Fig. S5 Electrocatalytic HER studies of MDS and X-MDS in alkaline medium (a) Nyquist plots, (b) ECSA calculations using plots of scan rate vs current density, (c) Before and after 1000 cycles of CN-MDS polarisation curves at a scan rate of 5 mV/s, and (d) J-T curve of CN-MDS for 100 h.

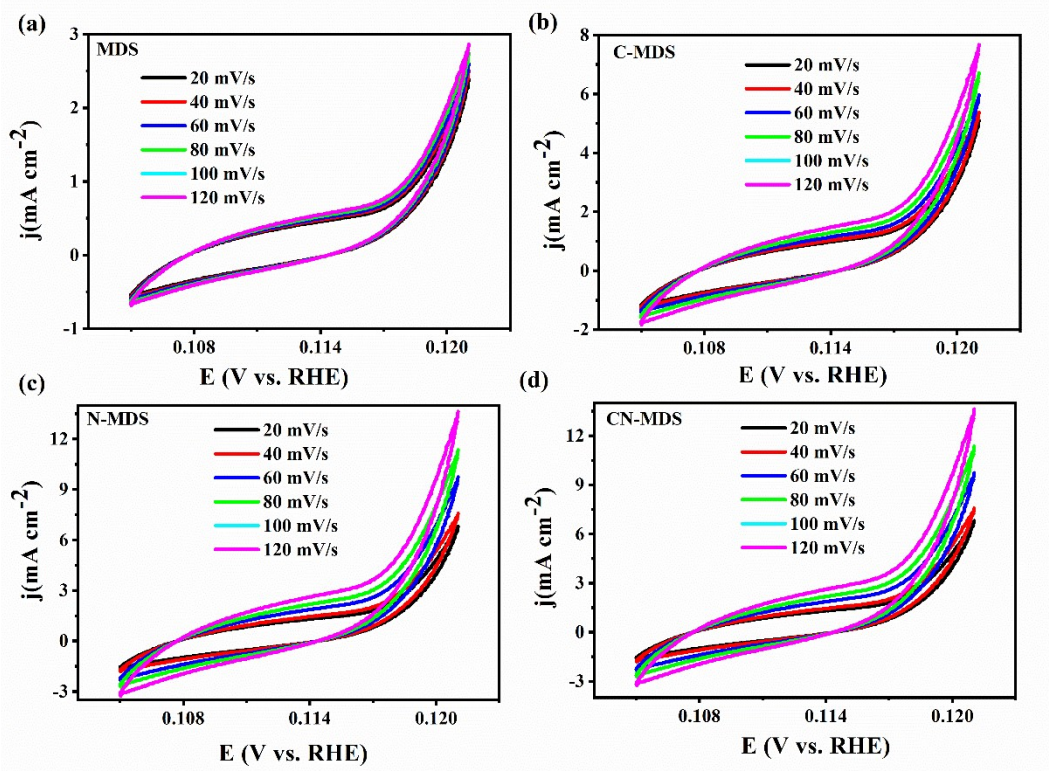

Fig. S6 Cyclic voltammograms for HER (a) MDS, (b) C-MDS, (c) N-MDS, and (d) CN-MDS in alkaline medium with the various scan rates.

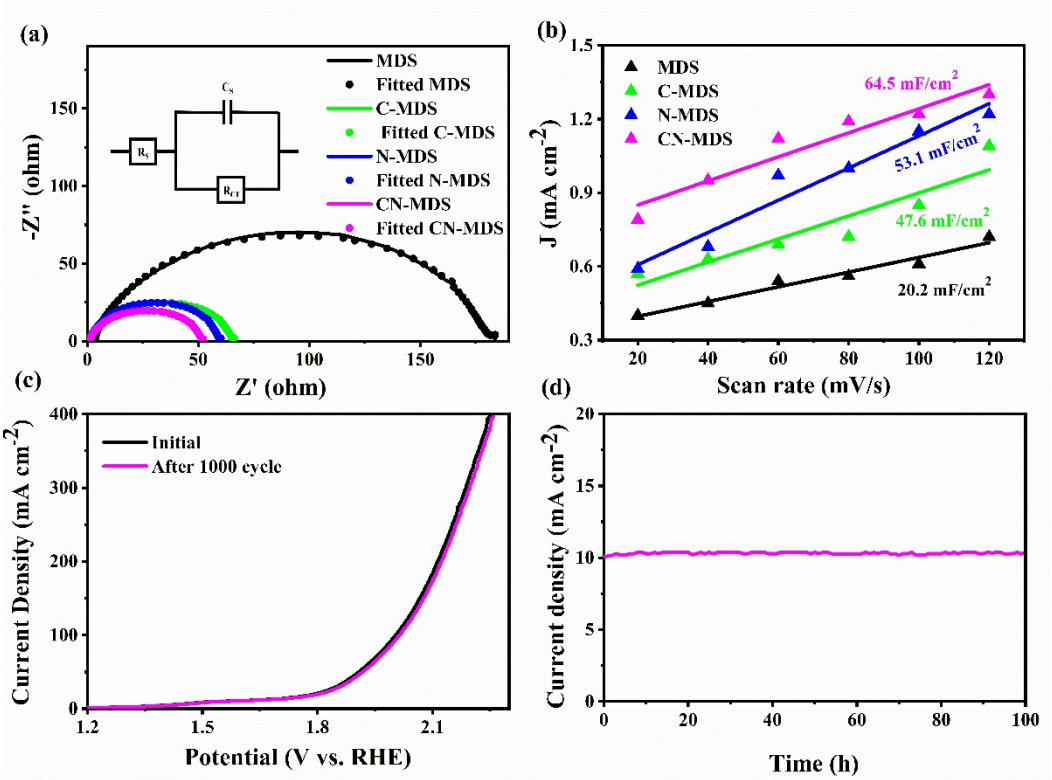

Fig. S7 Electrocatalytic OER studies of MDS and X-MDS in acid medium (a) Nyquist plots, (b) ECSA calculations using plots of scan rate vs current density, (c) Before and after

1000 cycles of CN-MDS polarisation curves at a scale rate of 5 mV/s, and (d) J-T curve of CN-MDS for 100 h.

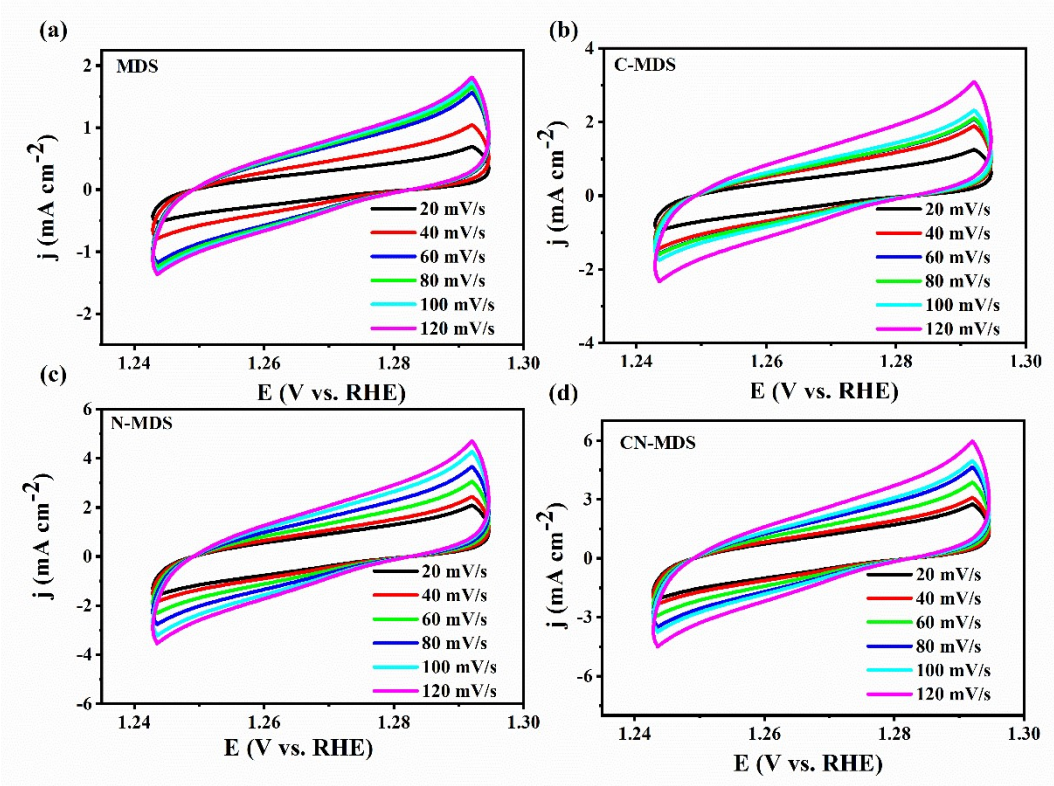

Fig. S8 Cyclic voltammograms for OER (a) MDS, (b) C-MDS, (c) N-MDS, and (d) CN-MDS in acid medium with the various scan rates.

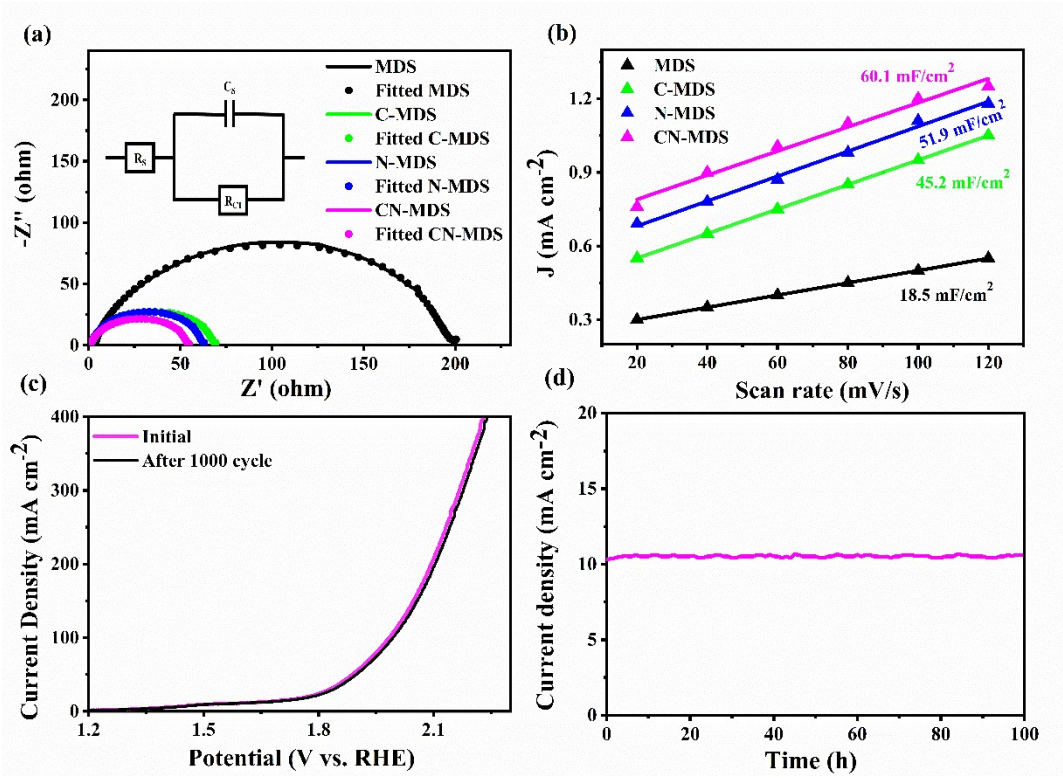

Fig. S9 Electrocatalytic OER studies of MDS and X-MDS in alkaline medium (a) Nyquist plots, (b) ECSA calculations using plots of scan rate vs current density, (c) Before and after 1000 cycles of CN-MDS polarisation curves at a scan rate of 5 mV/s, and (d) J-T curve of CN-MDS for 100 h.

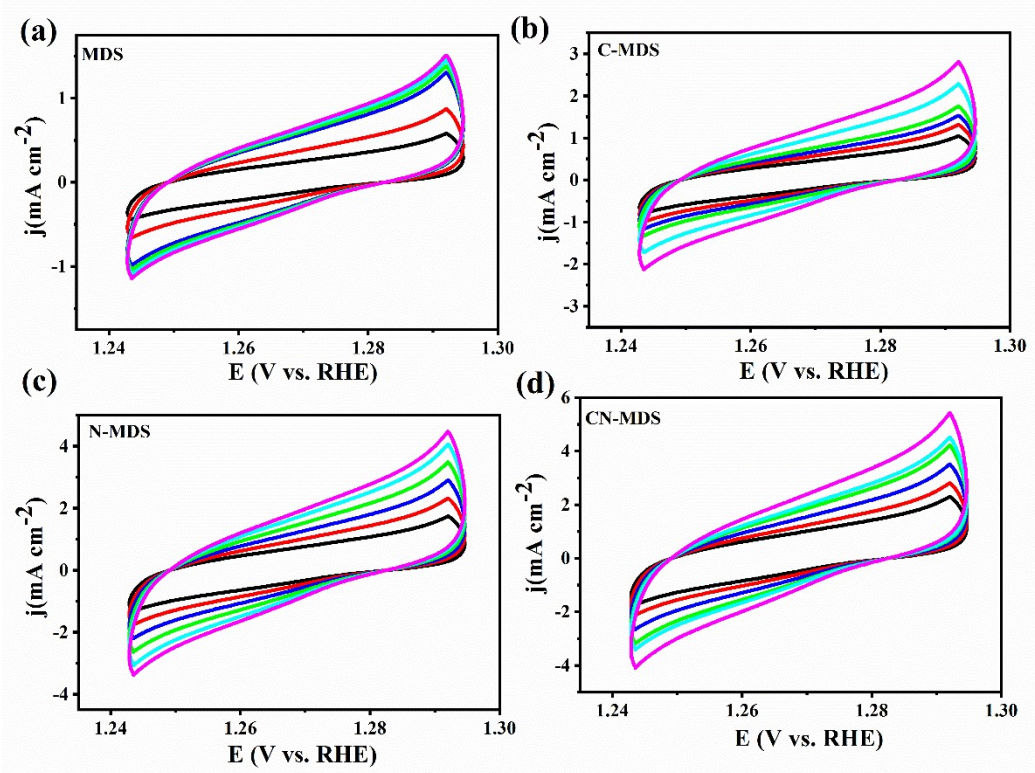

Fig. S10 Cyclic voltammograms for HER (a) MDS, (b) C-MDS, (c) N-MDS, and (d) CN-MDS in alkaline medium with the various scan rates.

OER stability test detail:

A CN-MDS NPs powder sample was coated onto nickel foam (NF) to enable reliable electrochemical characterization. Briefly, 1 mg of CN-MDS NPs was dispersed in a mixture of 320 µL ethanol/water (1:3, v/v) and 10 µL of 5 wt% Nafion solution. The resulting suspension was sonicated for 1 h to ensure uniform dispersion. Subsequently, 6 µL of the catalyst ink was drop-cast onto a freshly cleaned NF electrode (1 × 1 cm^2), which served as the working electrode. Electrochemical measurements were carried out using a conventional three-electrode configuration, with a platinum electrode as the counter electrode and an Ag/AgCl electrode as the reference electrode. Chronoamperometry (CA) was conducted for 100 h to evaluate stability, and SEM and XPS studies were subsequently carried out.

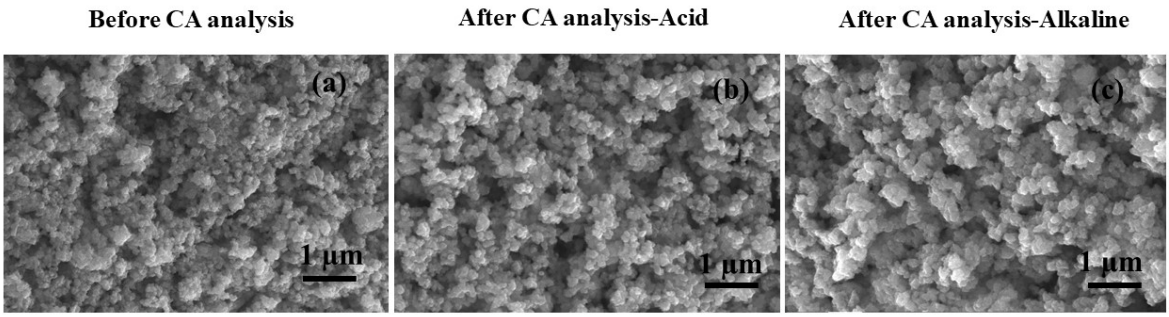

Fig. S11. SEM images of the CN-MDS catalyst (a) before the stability test, (b) after a 100 h OER stability test in an acidic medium, and (c) after a 100 h OER stability test in an alkaline medium.

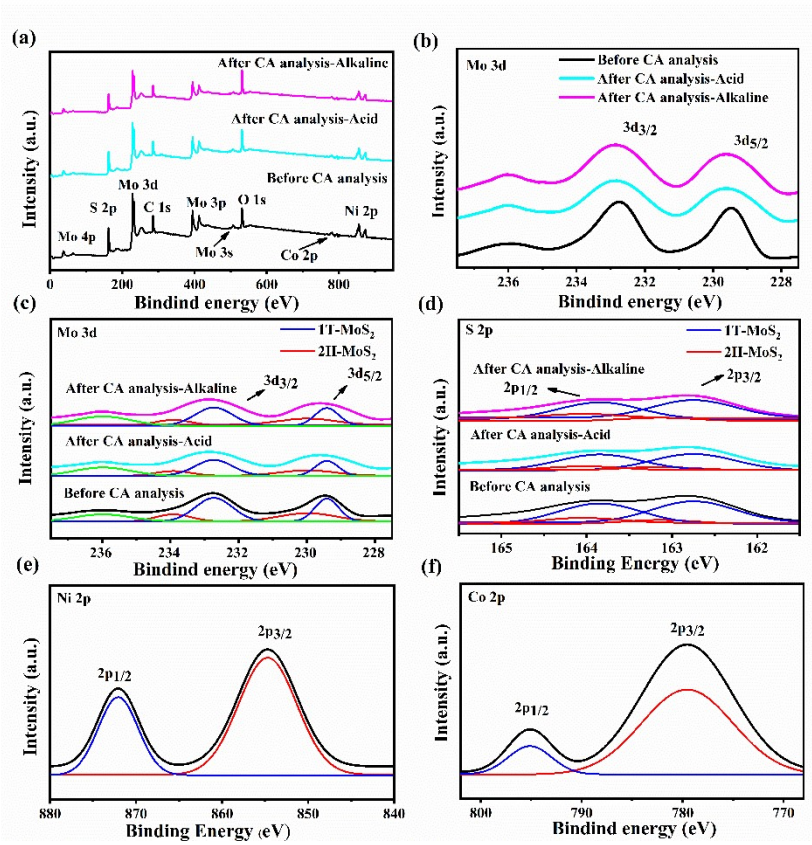

Fig. S12. XPS spectra of the CN-MDS catalyst before and after the 100 h of OER CA test: (a) full survey scan, (b) Mo 3d spectra, (c) deconvoluted Mo 3d spectra, (d) deconvoluted S 2p spectra, (e) deconvoluted Ni 2p spectra, and (f) deconvoluted Co 2p spectra.

After the OER stability test, the SEM images in Fig. S11 (b) and (c) show that the surface morphology remains essentially unchanged compared to Fig. S11 (a), indicating good structural stability of the catalyst. The XPS survey spectrum (Fig. S12 (a)) confirms the presence of Mo, S, Ni, Co, O, and C elements after the stability test. The high-resolution spectra

in Fig. S12 (c) and (d) reveal the coexistence of both metallic (1T) and semiconducting (2H) phases, demonstrating that the phase structure is retained during prolonged OER operation.

The results shown in Fig. S12 (a–d) further indicate that, after the prolonged 100 h stability test, the overall decrease in peak intensities arises from surface compositional changes caused by long-term electrochemical operation, particularly the formation of oxide and hydroxide species under OER conditions. This behavior is further supported by the Mo 3d spectra (Fig. S12 (b)). Compared with the spectra obtained before CA analysis, the Mo^{4+} $3d_{5/2}$ and $3d_{3/2}$ peak intensities decrease after CA, while a prominent peak appearing at 235.9 eV corresponds to Mo^{6+} species, indicating partial oxidation of Mo^{4+} during the OER process [1,2]. The emergence of Mo^{6+} species and the reduction in Mo^{4+} peak intensity confirm surface oxidation during stability testing, while the preserved morphology and phase structure collectively demonstrate the excellent electrochemical stability after the prolonged OER operation.

Table S2. Comparison of HER, OER, and overall performance at a current density of 10 mA cm^{-2}.

Catalysts	**HER**		**OER**		**Overall potential (V)**	**Medium**	**References**
	Potential (mV)	**Tafel slope (mV dec^{-1})**	**Potential (mV)**	**Tafel slope (mV dec^{-1})**			
Ni/Co-1T/2H MoS_2	84/91	42/48	232/240	55/57	1.5/1.52	Acid/alkaline	**This work**
Co-1T/2H MoS_2	167	61	263	68	1.54	Alkaline	[3]
1T-MoS_2/CoOOH	160	42	264	59	1.6	Acid	[4]
Ni-1T/2H MoS_2	117	102	250	43	1.36	Alkaline	[5]
Co-VS_2/MoS_2 NF	73.4	47.4	161.3	-	1.53	Alkaline	[1]
Co-MoS_2	130	126	200	174.8	1.86	Alkaline	[6]
$(ZnNiFeY)_xO_y$/MoS_2	214	69	308	115	1.65	Alkaline	[7]
Pani-MoS_2-Ni	159	40	175	42	-	Acid	[8]
N-rGO-MoS_2-	223	86	271	107	1.57	Alkaline	[9]

$Ni(OH)_2$							
MoS_2/NiS_2	131	84	278	91	1.59	Acid	[10]

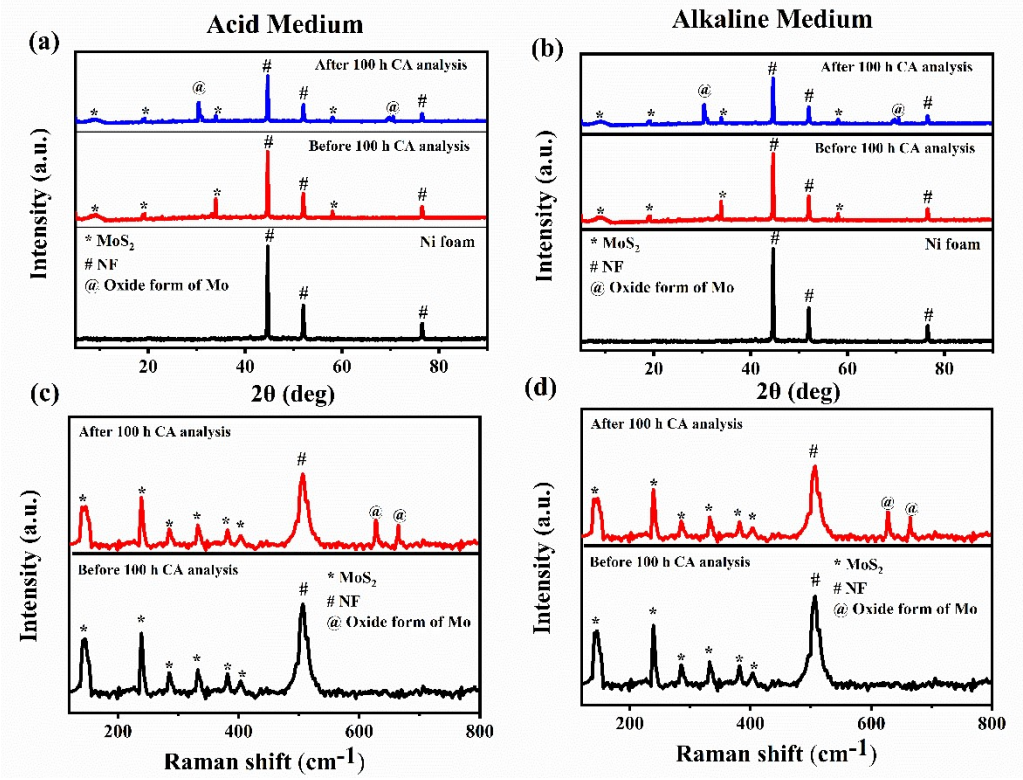

Fig. S13 (a) and (b) XRD patterns of CN-MDS NF and (c) and (d) Raman spectra of CN-MDS NF before and after overall water splitting electrolysis test.

Faradic efficiency calculation:

The faradic efficiency is one of the key components to calculate the hydrogen/oxygen conversion efficiency, and it was calculated using the following equation (1):

$$FE\% = \frac{n \times z \times F}{J \times A \times t} \times 100 ----(1)$$

Where z is the number of electrodes (z=2), F is the Faradic constant (F=96485 C/mol), J is the current density (50 mA/cm^2), A is the area of the electrode (A=1 cm^2), t is the time (t=25 hour) and n is the no. of mole of H_2 and O_2 calculated from the equation (2):

$$n = \frac{I \times t}{R \times F} ----(2)$$

Where I is the current in amperes, and R is the factor from the stoichiometry of the reaction (HER =2, OER=4) [3,11].

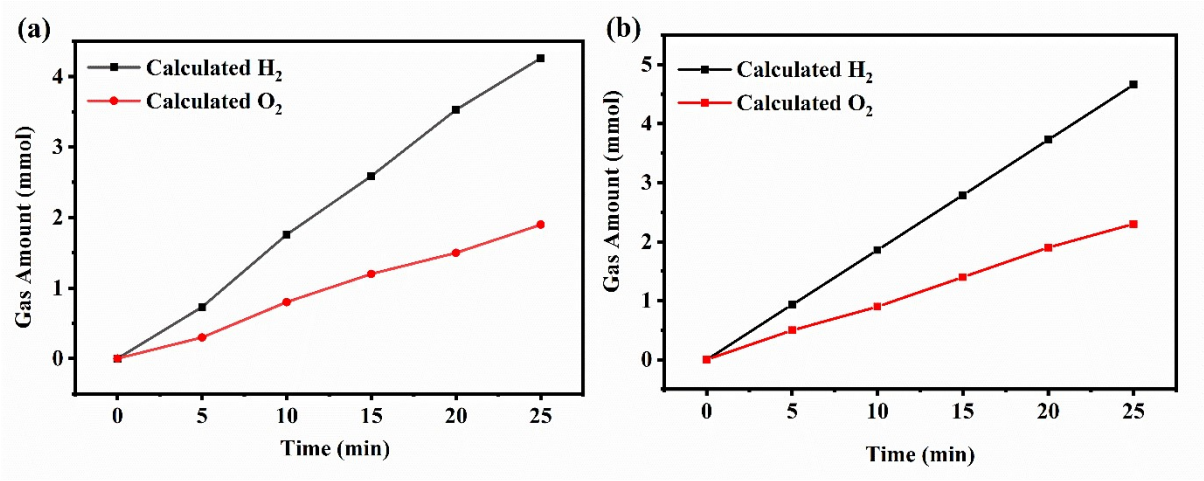

Fig. S14 Volumes of H_2 and O_2 theoretically measured at 10 mA cm^{-2} in acid and alkaline media.

Reference

1 P. Yin, T. Feng, T. Lei and W. Fu, *ACS Appl. Energy Mater.*, 2024, **7**, 11996–12003.

2 G. Helal, Z. Xu, W. Zuo, Y. Yu, J. Liu, H. Su, J. Xu, H. Li, G. Cheng and P. Zhao, *RSC Adv.*, 2024, **14**, 10182–10190.

3 P. Gurusamy, S. V. Perumalsamy, T. Pandian, G. Vellingiri, J. Kulanthaivel, S. Sinthika and K. M. Mithra, *Int. J. Hydrog. Energy*, 2025, **130**, 452–461.

4 B. Shang, P. Ma, J. Fan, L. Jiao, Z. Liu, Z. Zhang, N. Chen, Z. Cheng, X. Cui and W. Zheng, *Nanoscale*, 2018, **10**, 12330–12336.

5 P. Gurusamy, S. V. Perumalsamy, P. Gnanasekar, J. Kulandaivel, T. Paramasivam and T. Pandian, *Int. J. Hydrog. Energy*, 2024, **77**, 244–252.

6 W. Liu, L. Fu, S. Yang, Y. Lu, M. Li, L. Zhang and J. Tang, *ACS Omega*, 2025, **10**, 15129–15142.

7 S. C. Pathan, J. S. Shaikh, N. S. Shaikh, V. Márquez, M. Rittiruam, T. Saelee, P. Khajondetchairit, S. S. Mali, J. V. Patil, C. K. Hong, P. Praserthdam and S. Praserthdam, *South Afr. J. Chem. Eng.*, 2024, **48**, 425–435.

8 D. Saha, A. Bhardwaj, J. Wang, V. Pande, R. Hengstebeck, P. Bai and J. J. Watkins, *ACS Appl. Mater. Interfaces*, 2024, **16**, 42254–42269.

9 S. Debata, S. Banerjee and P. K. Sharma, *Electrochimica Acta*, 2019, **303**, 257–267.

10 J. Lin, P. Wang, H. Wang, C. Li, X. Si, J. Qi, J. Cao, Z. Zhong, W. Fei and J. Feng, *Adv. Sci.*, 2019, **6**, 1900246.

11 P. Gnanasekar, M. K. Eswaran, G. Palanichamy, T. K. Ng, U. Schwingenschlögl, B. S. Ooi and J. Kulandaivel, *ACS Sustain. Chem. Eng.*, 2021, **9**, 8572–8580.